One-chip analogue circuits for a new type of plasma wave receiver onboard space missions

Takahiro Zushi[1], Hirotsugu Kojima[1], Hiroshi Yamakawa[1]

[1]Research Institute for Sustainable Humanosphere, Kyoto University, Kyoto, 611-0011, Japan

5   *Correspondence to*: Hirotsugu Kojima (kojima.hirotsugu.6m@kyoto-u.ac.jp)

Abstract. Plasma waves are important observational targets for scientific missions investigating space plasma phenomena. Conventional fast Fourier transform (FFT)-based spectrum plasma wave receivers have the disadvantages of a large size and a narrow dynamic range. This paper proposes a new type of FFT-based spectrum plasma wave receiver that overcomes the disadvantages of conventional receivers. The receiver measures and calculates the whole spectrum by dividing the

10   observation frequency range into three bands: bands 1, 2, and 3, which span 1 Hz to 1 kHz, 1 to 10 kHz, and 10 to 100 kHz, respectively. To reduce the size of the receiver, its analog section was realized using application-specific integrated circuit (ASIC) technology, and an ASIC chip was successfully developed. The dimensions of the analog circuits were 4.21 mm × 1.16 mm. To confirm the performance of the ASIC, a test system for the receiver was developed using the ASIC, an analog-to-digital converter, and a personal computer. The frequency resolutions for bands 1, 2, and 3 were 3.2, 32, and 320 Hz

15   respectively, and the average time resolution was 384 ms. These frequency and time resolutions are superior to those of conventional FFT-based receivers.

1 Introduction

Space is filled with collisionless plasmas. Because space plasmas exchange their kinetic energies through plasma waves, the measurement of plasma waves is essential in understanding the physical processes occurring in space; thus, plasma wave

20   receivers have been used on past scientific satellites focused on the investigation of space plasma phenomena (cf. Gurnett, 1988).

Plasma wave receivers are categorized into two types, spectrum and waveform receivers, according to the form of their output data (Kojima, 2013). Spectrum receivers provide the intensities of frequency spectra, and waveform receivers output all wave properties, including their phases, except for the wavenumber. The waveform receiver instrument onboard the

25   GEOTAIL spacecraft shows its significance by contributing to the discovery of the nonlinear waveforms, so called Electrostatic Solitary Waves (Matsumoto et al., 1994). For this reason, a waveform receiver has become common in scientific missions; however, waveform observation should be intermittent because it produces a large amount of waveform data relative to the capacity of the satellite telemetry. Thus, spectrum receivers are still required to obtain consecutive observation data, and these types of receivers are complementary to each other.

Classical spectrum receivers based on analog circuits require large mass resources and power budgets. This disadvantage has led to the recent trend of not including the dedicated analog spectrum receiver onboard spacecraft. Instead, the frequency spectra are generated from waveform receiver data by a fast Fourier transform (FFT) performed by the onboard digital processing unit. This means that the waveform receiver simultaneously provides waveform and spectrum data; however, the waveform receiver has one disadvantage in its receiver gain setting. The waveform receiver should cover a wide frequency range without any frequency gaps using a single receiver. Because natural plasma waves in space show the feature that their spectral densities are larger in low frequency range than in high frequency range, the gain of the waveform receiver must be adjusted to the wave intensity at a low-frequency range to avoid saturating the receiver. This condition leads to the disadvantage of the waveform receiver having poor observation capabilities for relatively weak plasma waves in high frequency range. Another disadvantage of the waveform receiver is its power consumption. The sampling frequency must be set based on the highest observation frequency to be detected by the receiver. By the sampling theorem, the sampling frequency of the receiver should be at least double the highest frequency of the receiver. This means high-frequency sampling is required even to obtain the spectrum of low-frequency waves in the frequency band. However, the accompanying increase in power consumption is inevitable. Furthermore, when the frequency spectrum is obtained with a good frequency resolution, the onboard digital processing unit must process a huge amount of waveform data. This requires a high-performance digital processing unit, leading to further increases in the necessary resources, such as the power and size of the receiver.

This paper proposes a new type of small spectrum receiver for future space missions. The proposed receiver overcomes the disadvantages of conventional spectrum receivers regarding the size of the analog circuit. Additionally, this receiver is based on waveform receivers using the same type of onboard FFT processing as in recent space missions. The observed waveforms are limited in several frequency bands through filters with different cutoff frequencies in front of the main amplifiers. Furthermore, the sampling frequencies of the analogue-to-digital converters (ADCs) and the gains of the main amplifiers change synchronously with the changes in the filters. This synchronization enables the measurement of plasma waves in an appropriately defined receiver dynamic range with a reasonable power consumption. The realization of the above function requires a large amount of mass and size resources in composing the boards using discrete electrical devices because several independent filters and control circuits must be prepared for the synchronization. To resolve this resource issue, an application-specific integration circuit (ASIC) chip, which contains all of the analog components for the proposed spectrum receiver, was developed. The size of the circuit implemented inside the chip is 4.21 mm × 1.16 mm for three frequency bands. The present paper introduces the design and specifications of the proposed spectrum receiver and demonstrates its performance based on the experimental results of the developed chip.

2 New type of the FFT based spectrum receiver

Conventional spectrum receivers are categorized into three types: sweep frequency analyzers (SFAs), multichannel analyzers (MCAs), and FFT-based receivers (Kojima, 2013). The SFA is a type of heterodyne receiver that provides narrow-band frequency spectra, and its observation frequency is changed by sweeping the frequency of the local oscillator for frequency

5 conversions. The converted output signal is rectified before it is input into the ADC. The MCA is composed of a group of bandpass filters (BPFs) with different center frequencies. The output signals of the BPFs are amplified and rectified before they are sampled in parallel. The SFA provides spectra with a high frequency resolution, whereas the MCA provides spectra with a high time resolution. The SFA and the MCA have been adopted in combination in many past space missions because they complement each other in terms of their resolutions for the observed spectra. The SFA and MCA are generally

10 composed of independent receivers with different frequency bands. This allows the gain to be set independently in each frequency band considering the signal dynamic range; however, because they require a large amount of resources in their analog circuits, recent space missions have adopted FFT-based spectrum receivers.

The FFT-based spectrum analyzer is based on a waveform receiver. Digitized waveform data at the ADC are fed to a digital processing unit, such as a central processing unit (CPU) and a digital signal processor. The digital processing unit computes

15 the FFT to generate a frequency spectrum. The FFT-based spectrum analyzer has the advantage of low mass and size resource requirements. The progress of digital technologies allows the realization of real-time FFT calculations using software or a field-programmable gate array (FPGA) without requiring a large amount of mass and size resources. This is why many recent missions have used FFT-based spectrum analyzers (Kasaba et al., 2010; Kletzing et al., 2013). The analog part of the FFT-based spectrum analyzer is shared with a waveform receiver. The design of the analog circuit is very simple;

20 however, its disadvantages, which originate from the wideband receiver, are the same as those of the waveform receiver regarding the setting of the dynamic range and the need for sufficient high-frequency sampling to avoid aliasing.

The insertion of several filters with different cutoff frequencies in front of the main amplifier resolves the above problems caused by the wide-band amplification. Figure 1(a) shows a block diagram of the proposed spectrum receiver. The most important point in this block is the presence of the band-limiting filters in the first stage. The cutoff frequencies of the band-

25 limiting filters can be changed using an external control signal. Furthermore, the sampling frequency, the cutoff frequency of the antialiasing filter, and the gain of the main amplifier also change synchronously with the change in the cutoff frequency of the band-limiting filter. This means that the observation frequency band can be changed stepwise over time by changing the external signal and that waveforms limited in different frequency bands can be obtained when the gain of the receiver is set to appropriate values.

30 Because the proposed spectrum receiver requires additional filters with cutoff frequencies different from those of conventional FFT-based receivers, its analog circuit is much larger than that of a typical FFT-based spectrum receiver. To solve this problem, an ASIC chip for the analog circuit of the proposed receiver was developed. The developed ASIC contains the following components: a band-limiting filter, an antialiasing filter, and a main amplifier. Because the receiver

applies band limiting, it should switch among several frequency bands over time to obtain a wide-band spectrum. In the design of the proposed receiver, the observation frequency range was from 1 Hz to 100 kHz, and the receiver switches among three bands: bands 1, 2, and 3 spanning 1 Hz to 1 kHz, 1 to 10 kHz, and 10 to 100 kHz, respectively. The receiver changes the observation frequency band by altering the cutoff frequency of the band-limiting filters via the external control

5 signal. A schematic of the frequency response of the band-limiting filter is also shown in Figure 1(b). In addition to the cutoff frequency of the band-limiting filter, the gain of the main amplifier, the cutoff frequency of the antialiasing filter, and the sampling frequency can be changed by varying the external signal. The details of the ASIC design and performance are described in the following section.

The digital processing unit, which could be an FPGA or a CPU, has two roles. The first is to control the analog circuit and

10 change the sampling frequency through the controller circuit included in the ASIC, and the second is to calculate the frequency spectrum using a FFT.

3 Application-specific integration circuit for the analog circuit of the receiver

Figure 2 shows a detailed block diagram of the ASIC developed for the analog circuit of the new type of plasma wave receiver. The ASIC consists of four blocks indicated by different colors in Figure 2: the band-limiting filter, main amplifier,

15 antialiasing filter, and control blocks.

The band-limiting block is the most essential block in the developed spectrum receiver. It is composed of two Gm-C filters: a second-order Butterworth high-pass filter (HPF) and a second-order Butterworth low-pass (LPF). The cutoff frequency of the LPF is 100 kHz, and that of the HPF can be set to 1 or 10 kHz using the external control signal. Depending on the temporal distribution of the observation bands, the combination of these filters changes. For band 1, the signal from the

20 preamplifiers passes through only the LPF. For bands 2 and 3, the signals are filtered by both the HPF and LPF, and the cutoff frequency of the HPF is set to 1 and 10 kHz, respectively. As a result, the band-limiting filter works as an LPF for band 1, and as a BPF for bands 2 and 3. The role of the band-limiting filter is to eliminate all signals except for the target frequency range in each band to prevent amplifier saturation by unnecessary signals. It is desirable for the cutoff frequencies of the LPF to be 1, 10, and 100 kHz for bands 1, 2, and 3; however, LPFs with cutoff frequencies of 1 and 10 kHz occupy a

25 large space because they require large capacitors. Because the intensity of plasma waves decreases as the frequency increases, only the cutoff frequency of the HPF should be altered, and the fixed cutoff frequency of the LPF is 100 kHz.

Figure 3 shows the circuit diagram of the Gm-C HPF used in the band-limiting block. Because the filter is fully differential, the circuit structure is symmetric. The Gm-C filter is a continuous time filter composed of operational transconductance amplifiers (OTAs) and capacitors. The OTA is an amplifier with an output current that is proportional to the differential

30 input voltage. The characteristics of the OTA are represented by the transconductance g_m, and the input voltage V_{IN} and output current I_{OUT} are related as $I_{OUT} = g_m \cdot V_{IN}$. The frequency response of the filter is determined by the

Geoscientific
Instrumentation
Methods and
Data Systems
Discussions

transconductances of the OTAs and the capacitances. The three OTAs contained in this filter have the same transconductance of 0.5 µS. The transfer function and cutoff frequency are respectively expressed as

$$H_{\text{GmCHPF}}(s) = \frac{\frac{2C_1}{C_1+C_3}s^2}{s^2+\frac{2gm}{C_1+C_3}s+\frac{4g_m^2}{C_2(C_1+C_3)}}, \tag{1}$$

$$f_{\text{cHPF}} = \frac{1}{\pi}\frac{g_m}{\sqrt{C_2(C_1+C_3)}}, \tag{2}$$

where s is a complex number frequency parameter and C_n are the capacitances. The capacitance C_1 is the total capacitance of the changeable capacitor composed of a switch S_1 and two capacitors C_{11} and C_{12} in parallel, as shown in Figure 3; C_2 is defined in a similar manner. The changeable capacitors C_1 and C_2 allow the filter to change the cutoff frequency. Table 1 gives the correspondence of the capacitances and switch configurations to the cutoff frequency. S_1 and S_2 change simultaneously and have the same state. The capacitance is determined based on the characteristic variation using circuit simulations.

The main amplifier has three gain steps: 0, 20, and 40 dB. These gain steps are independently selectable in each band considering the levels of the observed signals in each frequency band.

The block of the antialiasing filter consists of a sixth-order Chebyshev LPF and a second-order Butterworth LPF. The sixth-order LPF is the antialiasing filter used to sample the observed signal with the ADC. Because the antialiasing filter requires sharp reduction characteristics with an accurate cutoff frequency, a high-order switched capacitor (SC) filter was used. An SC filter is a discrete time filter using SC circuits. The sixth-order Chebyshev LPF is composed of three biquad LPFs. Figure 4 shows the circuit diagram for each stage. The transfer functions in each stage are expressed as

$$H_{\text{SCLPF,13}}(s) = \frac{-f_{\text{CK}}^3\frac{C_1C_4}{C_2C_6}}{s^2+f_{\text{CK}}\frac{C_4C_5}{C_2C_6}s+f_{\text{CK}}^3\frac{C_3C_4}{C_2C_6}}, \tag{3}$$

$$H_{\text{SCLPF,2}}(s) = \frac{-f_{\text{CK}}^3\frac{C_1C_4}{C_2C_6}}{s^2+f_{\text{CK}}\frac{C_5}{C_6}s+f_{\text{CK}}^3\frac{C_3C_4}{C_2C_6}}, \tag{4}$$

where f_{CK} is the clock frequency for switching. The capacitances of each capacitor used in this SC filter are given in Table 2. The frequency response of the SC filter is determined by the capacitance ratio and f_{CK}. In present design, the cutoff frequency of the sixth-order LPF is one-hundredth of the f_{CK}. The clock signal for the SC filter is generated by dividing the supplied clock signal with a frequency of 10 MHz. Because the prescaler is designed to allow the division ratio to be set to 1/100, 1/10, or 1, the cutoff frequency of the SC filter can be setAnother LPF in the block of the antialiasing filter is the noise reduction filter. Because the SC filter generates switching noise, the Gm-C LPF is used as a noise elimination filter. The circuit diagram of the noise elimination Gm-C LPF is shown in Figure 5. All OTAs have the same transconductance of 12 µS. The transfer function and the cutoff frequency are respectively expressed as to 1 kHz, 10 kHz, or 100 kHz.

$$H_{\text{GmCLPF}}(s) = \frac{\frac{g_m^2}{C_1C_2}}{s^2+\frac{g_m}{C_2}s+\frac{g_m^2}{C_1C_2}}, \tag{5}$$

$$f_{\text{cLPF}} = \frac{1}{2\pi}\sqrt{\frac{g_m^2}{C_1 C_2}}, \qquad\qquad (6)$$

In a manner similar to the Gm-C HPF, the capacitances C_1 and C_2 represent the total capacitances of the changeable capacitor composed of two switches and three capacitors in parallel. The cutoff frequency can be set to 4, 40, or 400 kHz. Table 3 gives the correspondence of the capacitances and switch configurations to the cutoff frequency. S_{11} and S_{12} change

5   simultaneously and have the same state, and S_{21} and S_{22} change in a similar manner.

The controller consists of two prescalers and logic gates. One prescaler supplies the clock signal for the SC filter, and the other supplies the sampling clock to the ADC. The frequency of the clock signals fed to each prescaler is 10 MHz. The division ratios of the prescaler for the sampling clock are 1/3000, 1/300, and 1/30. The role of the logic gates is to supply logic signals to each component depending on the input of the controller, which indicates the observation band. Table 4 lists

10   the correspondence of the properties of each component to the observation band.

The above circuits were designed using a complementary metal–oxide semiconductor (CMOS) 0.25-µm mixed-signal process (Taiwan Semiconductor Manufacturing Company). Figure 6 shows the layout design of the ASIC. The dimensions of the circuits are 4.21 mm × 1.16 mm. The bonding wires connect to the pins through electrostatic discharge protection pads, which are located on the left of Figure 6.

15   Figures 7 and 8 show the frequency response and input equivalent noise density of the developed ASIC, respectively. The gain ripples near each upper cutoff frequency are the result of the response of the Chebyshev filter. The observed gains for each band and gain settings are given in Table 5. The gains of the passband in band 3 are less than those in bands 1 and 2 and by a few decibels. This drop in the gain is a result of the band-limiting filters. The noise level in the passband is less than −100 dB V Hz$^{-1/2}$ under almost all gain and observation band configurations.

20   As described above, the external signal controls each component inside the ASIC to change the observation band. Changing the observation band changes the following properties: the cutoff frequencies of the band-limiting filter and antialiasing filter, the switch determining whether the HPF is applied, and the gain of the main amplifier. This process may cause unwanted transient circuit responses at the timing of changing observation bands. Because it is impossible to avoid the unwanted transient responses, observation data obtained within a transient state must be discarded. Thus, the settling time must be

25   determined. The transient response of third component of the SC filter has the largest amplitude because it has the highest Q factor among the analog components, and the dumping time constant of the responses depends on the cutoff frequency of the SC filter. The settling times for bands 1, 2, and 3 were determined to be 10 ms, 1 ms, and 100 µs, respectively, based on the observation results. The frequency of the transient response is almost the same as the cutoff frequency of the SC filter.

4 Performance of the proposed spectrum receiver using the application-specific integrated circuit

30   To confirm the performance of the developed ASIC, a test system was developed, as shown in Figure 9. The proposed plasma wave receiver consists of the analog components incorporated in the ASIC and a digital processing unit, such as a

CPU or FPGA. In the test system for the ASIC, a personal computer (PC) running the Widows 7 operating system with an ADC was used to model the digital processing unit. AIO-121602LN-USB (CONTEC Co., Ltd.) was used as the ADC. The program running on the PC controls the switching timing of each frequency band of the ASIC, the analog-to-digital conversion, and the data acquisition from the ADC. The PC also calculates the FFT to obtain the frequency spectra.

5   Figure 10 shows the measurement sequence inthe test system. The digital unit controls the switches inside the ASIC, and the ASIC outputs the band-limited waveforms in the time series of the corresponding frequency band. The time resolution of the receiver is the sum of the sampling time; the time spent waiting for the transient response to settle; and the FFT calculation time, which includes the time required to write the data to the hard drive. The waiting time for bands 1, 2, and 3 were determined to be 20, 2, and 1 ms respectively. The measurement time for each band depends on the sampling rate and the

10   number of data points. In the present test system, the number of data points is 1024, and the sampling rates for bands 1, 2, and 3 are 3.3, 33.3, and 333.3 kHz, respectively. Table 6 lists the measurement times and frequency resolutions for each band calculated from the configuration of the receiver.

Figure 11 shows the observation results in the test system. The input signal as a reference was a sinusoidal wave with a frequency of 100 Hz and an amplitude of 2 mV. The gain setting of the ASIC was 40 dB for all bands. The actual average

15   measurement time resolution was 383 ms. As described in Section 3, the frequencies of the transient responses for each observation band were almost the same as the cutoff frequencies of the SC filter. The results showed no transient response in each band, indicating that the settling times determined from the observation results and given at the end of Section 3 were accurate. Generally, the demonstration model using the ASIC functioned correctly and had sufficient time and frequency resolution.

20   The power consumption of the ASIC containing the above one channel new type of spectrum receiver is 36 mW. This power consumption is very low relative to the analogue circuits of other plasma wave receivers. For the reference, the power consumption of one channel analogue circuit in the plasma wave receiver onboard the Japanese Geospace mission called ERG satellite is about 430 mW. Since the specification of the ERG plasma wave receiver is not identical to that of the ASIC, it is difficult to compare precisely the power consumptions of these two analogue circuits; however, the power consumption

25   of the ASIC is one-order smaller than that in the ERG satellite. This is the significant point of the ASIC receiver in the use of nano-satellites or cubesats.

5 Conclusion

This paper proposed a new type of FFT-based spectrum plasma wave receiver that allows miniaturization and overcomes the disadvantages of conventional receivers. The proposed receiver measures and calculates the whole spectrum by dividing the

30   observation frequency range into three bands: bands 1, 2, and 3, which span 1 Hz to 1 kHz, 1 to 10 kHz, and 10 to 100 kHz, respectively. The ASIC chip, which is the core component of the receiver, was successfully developed in this study. The size of the chip is 5 mm × 5 mm. Additionally, a demonstration model of the receiver was developed using the ASIC, an ADC,

and a PC. The observation results for the demonstration model were obtained and analyzed. The frequency resolutions for bands 1, 2, and 3 are 3.2, 32, and 320 Hz, respectively, and the average time resolution is 383 ms. These frequency and time resolutions are superior to those for conventional FFT-based receivers. Though the demonstration model used a PC, it is expected that a receiver without a PC can be realized using a digital signal processor or FPGA, which can calculate the FFT

5   as rapidly as a PC can. Consequently, the proposed FFT-based receiver can be effectively miniaturized and overcomes the problems caused by wide-band amplification.

Although the waveform and spectrum receivers are complementary, recent space missions have used only waveform receivers because of the severe resource restrictions of the satellites, and spectral data have then been calculated from the waveform data. Such waveform-based spectrum receivers allows the size of the receiver to be reduced; however, they have

10   the same disadvantages as waveform receivers. The proposed spectrum receiver overcomes these disadvantages by using the ASIC, which includes analog circuits. In addition, the proposed spectrum receiver is small enough to allow the independent use of both the waveform and spectrum receivers in a satellite. Furthermore, from the perspective of using microsatellites in space science missions, the size of the receiver is important.

The miniaturized analog circuit allows the realization of more sophisticated observation systems for plasma waves. As

15   described in Section 2, the proposed spectrum receiver requires a digital processing unit, such as an FPGA or CPU, to calculate the frequency spectrum, and the waveform receiver also requires such a unit to compress waveform data and thus effectively transfer observation data.

Finally, an analog / digital mixed ASIC has the capability of realizing a one-chip plasma observation system. Once we implement on the chip, ADC and digital components such as FFT and data compression as well as the analog components

20   that are described in the present paper, the plasma wave observation system drastically becomes small. Since multiple channels of receivers can be installed on the same chip, the simultaneous observation of multiple components can be performed based on the one-chip system. This allows the drastic miniaturization of the receiver and decreases development costs because the ASIC has the advantage of easy mass-production. This will likely lead to increased observation opportunities and the realization of new observation systems. Thus, the one-chip plasma observation system may be a major

25   breakthrough for plasma observation.

References

Gurnett, D. A., Principles of space plasma wave instrument design, Measurement techniques in space plasmas: Fields, Geophysical Monograph, 103, 121-136, 1998.

Kasaba, Y., Bougeret, J. L., Blomberg, L. G., Kojima, H., Yagitani, S., Moncuquet, M., Trotignon, J.G., Chanteur, G.,

5   Kumamoto, A., Kasahara, Y., Lichtenberger, J., Omura, Y., Ishisaka, K., Matsumoto, H.: The Plasma Wave Investigation (PWI) onboard the BepiColombo/MMO: First measurement of electric fields, electromagnetic waves, and radio waves around Mercury, Planetary and Space Science, 58(1-2), 238–278, doi:10.1016/j.pss.2008.07.017, 2010.

Kletzing, C. A., Kurth, W. S., Acuna, M., MacDowall, R. J., Torbert, R. B., Averkamp, T., Bodet, D., Bounds, S.R., Chutter, M., Connerney, J., Crawford, D., Dolan, J.S., Dvorsky, R., Hospodarsky, G.B., Howard, J., Jordanova, V., Johnson, R.A.,

10 Kirchner, D.L., Mokrzycki, B., Needell, G., Odom, J., Mark, D., Pfaff, R. Jr., Phillips, J.R., Piker, C.W., Remington, S.L., Rowland, D., Santolik, O., Schnurr, R., Sheppard, D., Smith, C.W., Thorne, R.M., Tyler, J.: The Electric and Magnetic Field Instrument suite and Integrated Science (EMFISIS) on RBSP, The Van Allen Probes Mission, 127–181, doi:10.1007/978-1-4899-7433-4-5, 2013.

Kojima, H.: Plasma wave receivers onboard scientific satellites, An introduction to Space Instrumentation, ed. K. Oyama and

15 F. Cheng, 227-240, 2013.

Matsumoto, H., Nagano, I., Anderson, R.R., Kojima, H., Hashimoto, K., Tsutsui M., Okada, T., Kimura, I., Omura, Y., Okada, M.: Plasma Wave Observations with GEOTAIL Spacecraft, J. Geomag. Geoelectr, 46, 59–95, 1994.
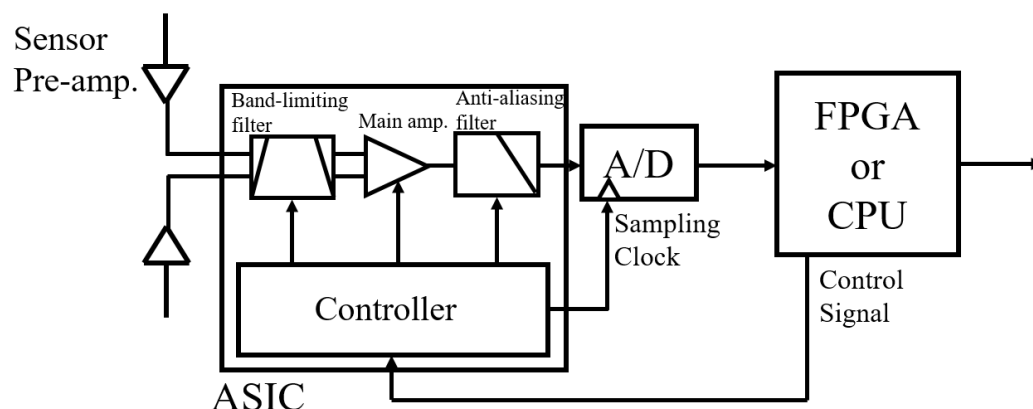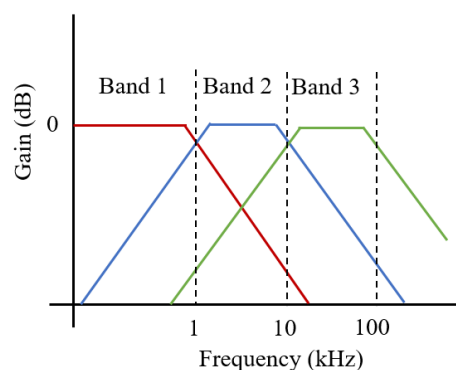
Figure 1: (a) Block diagram of the structure of the proposed FFT-based receiver. (b) Schematic of the frequency response of the band-limiting filter.
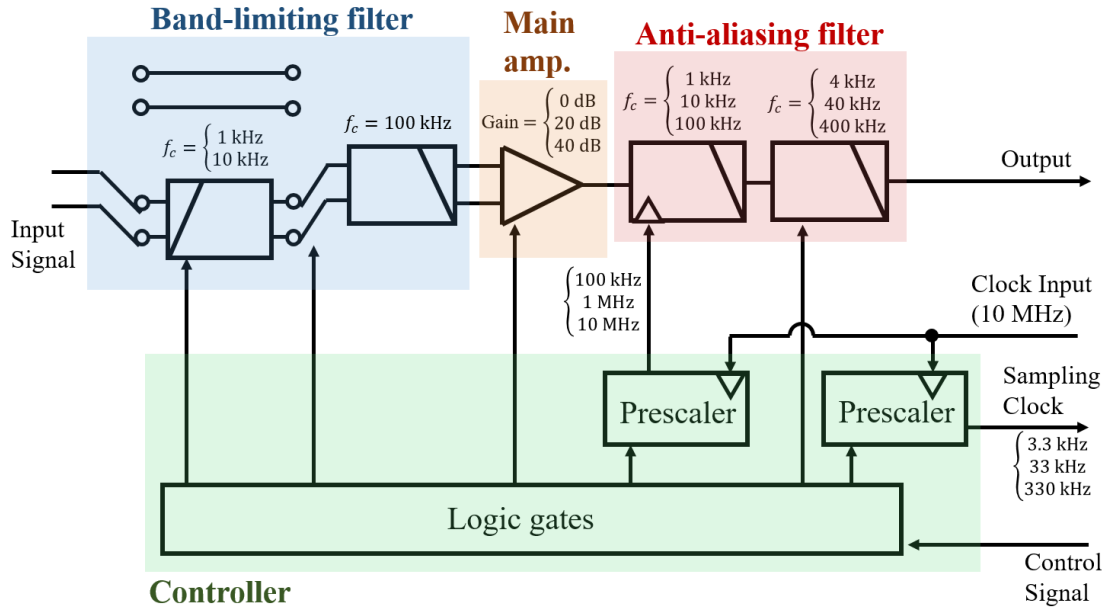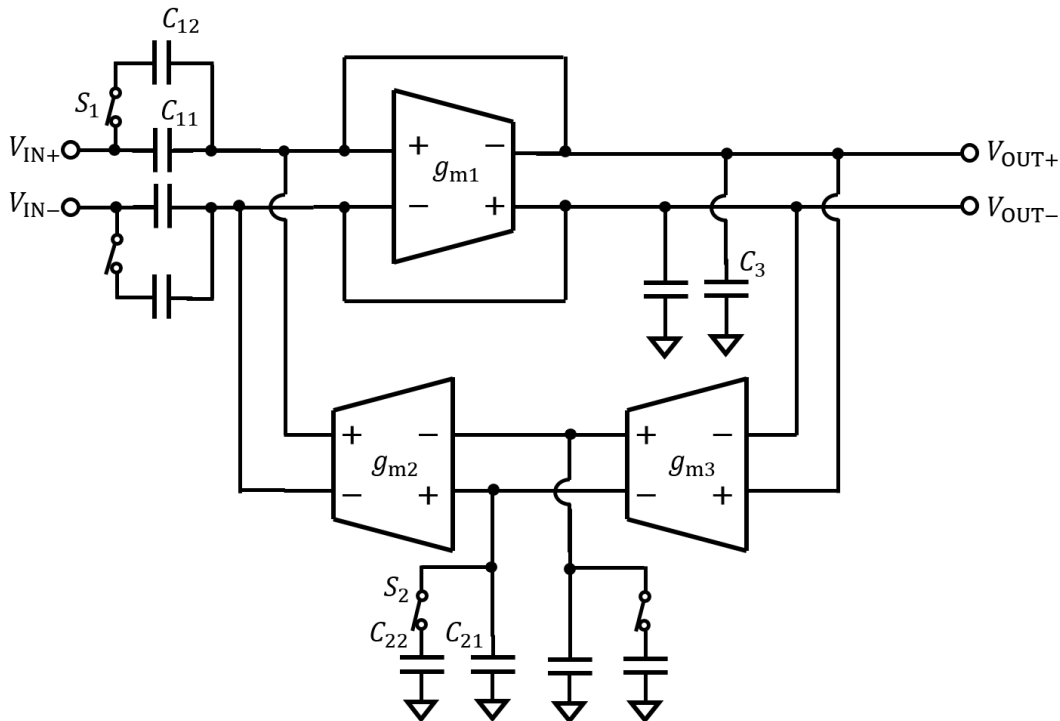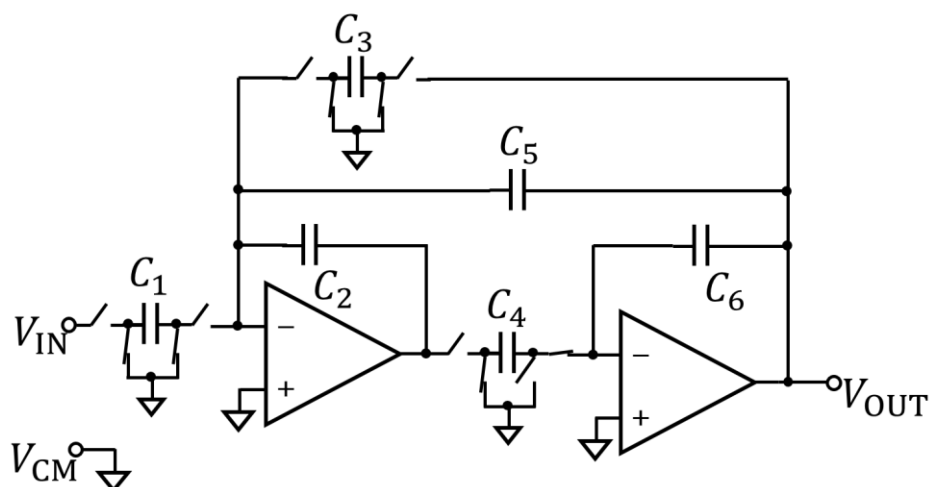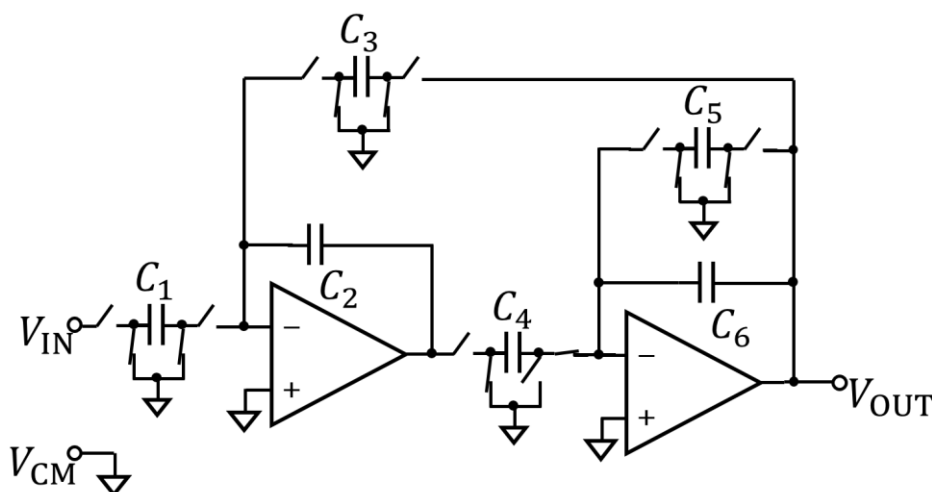
Figure 2: Block diagram of the ASIC.

5   Figure 3: Circuit diagram of the Gm-C HPF.

11

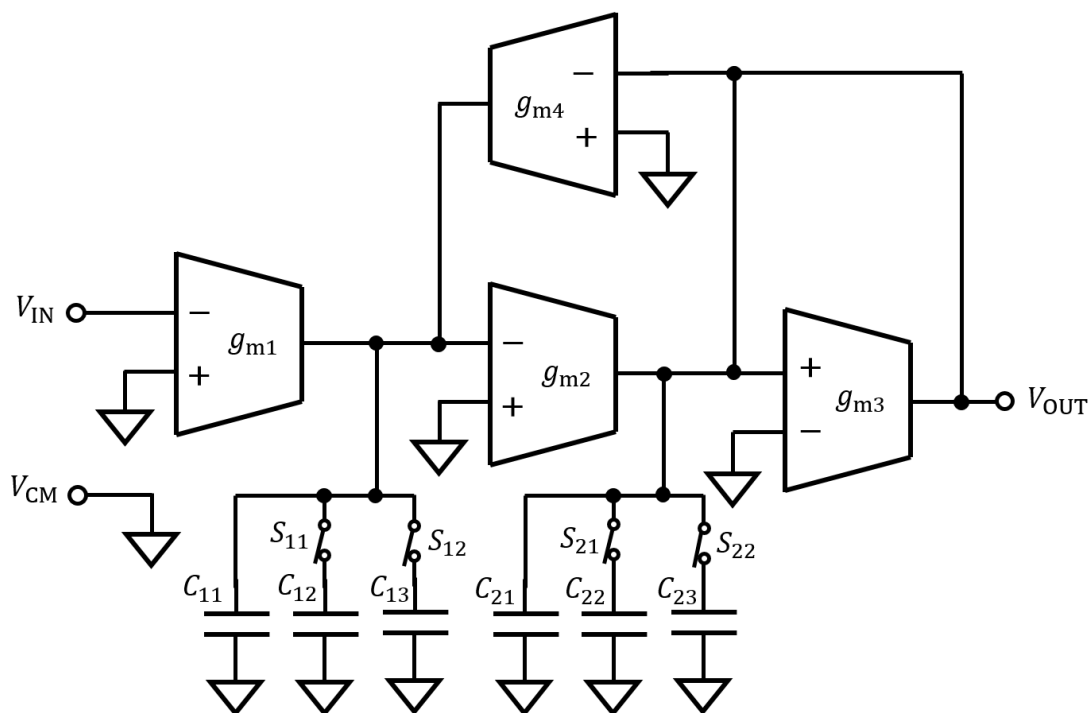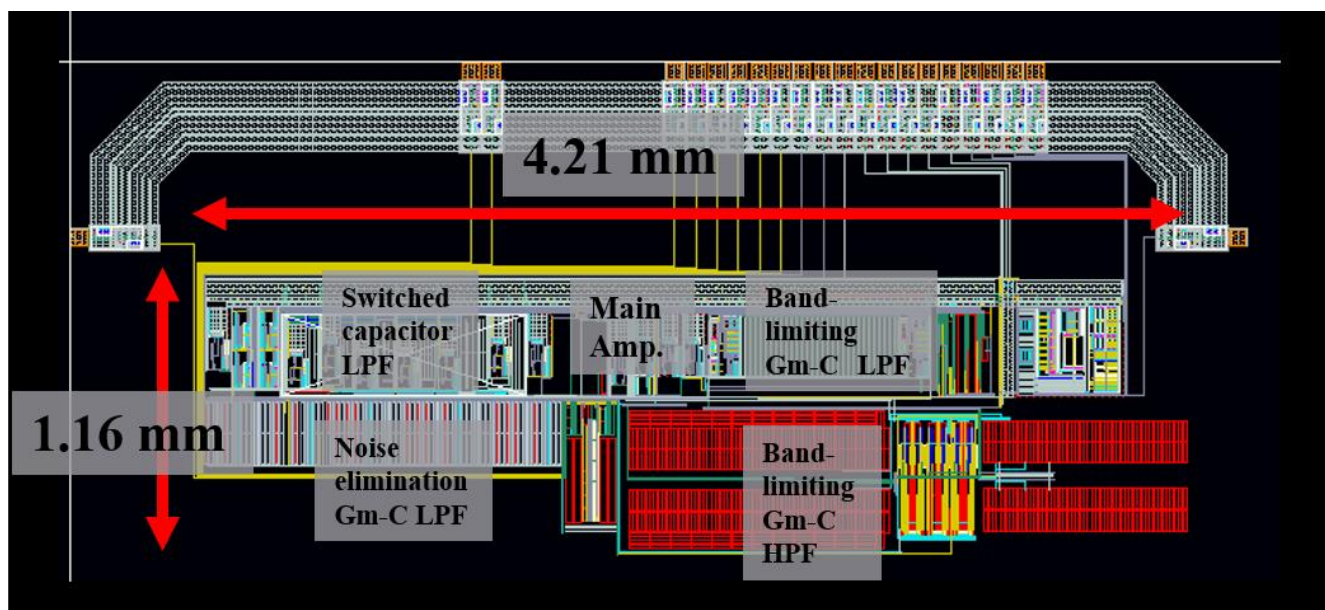Figure 4: Circuit diagram of the (a) first and third and (b) second stages of SC LPF.
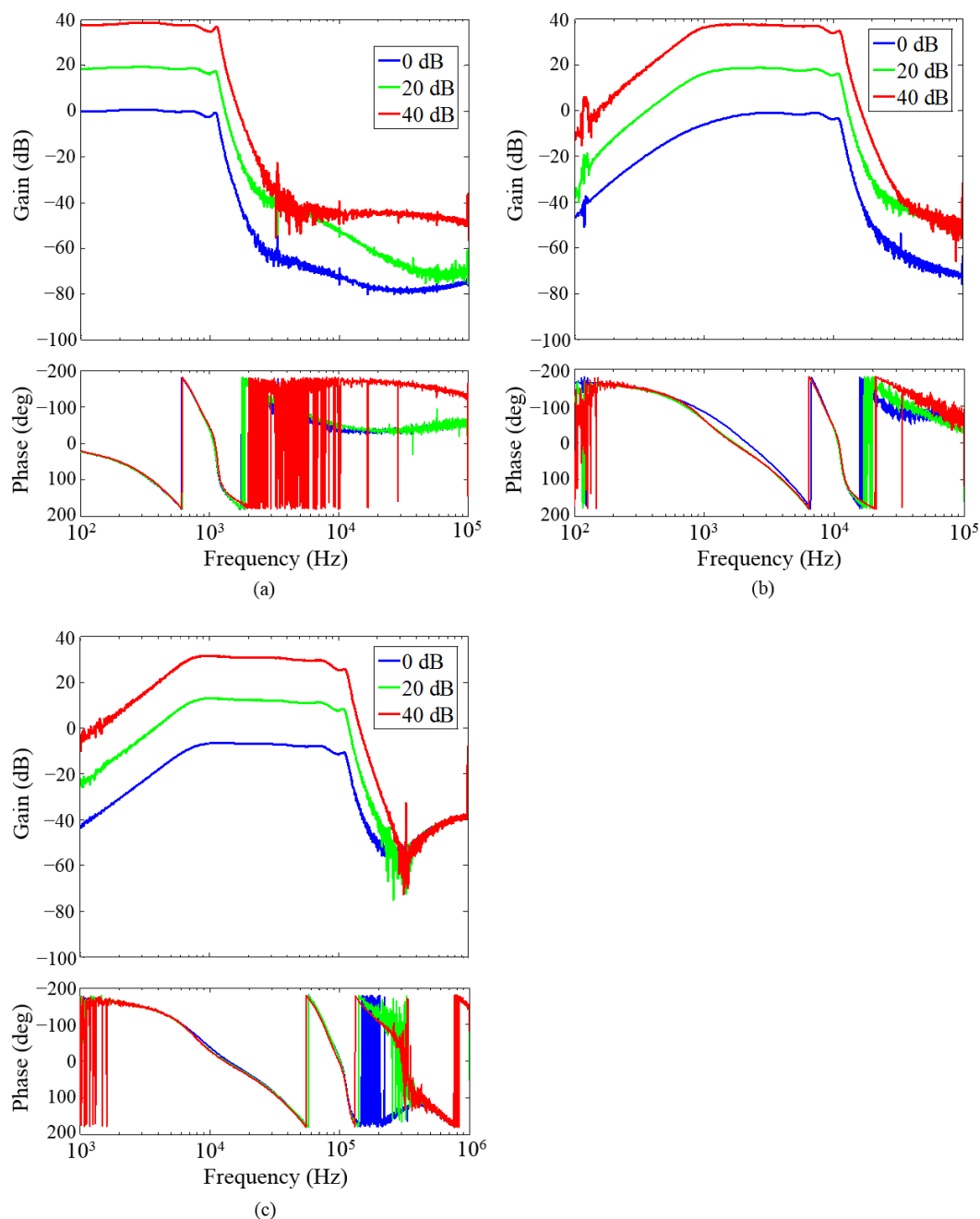
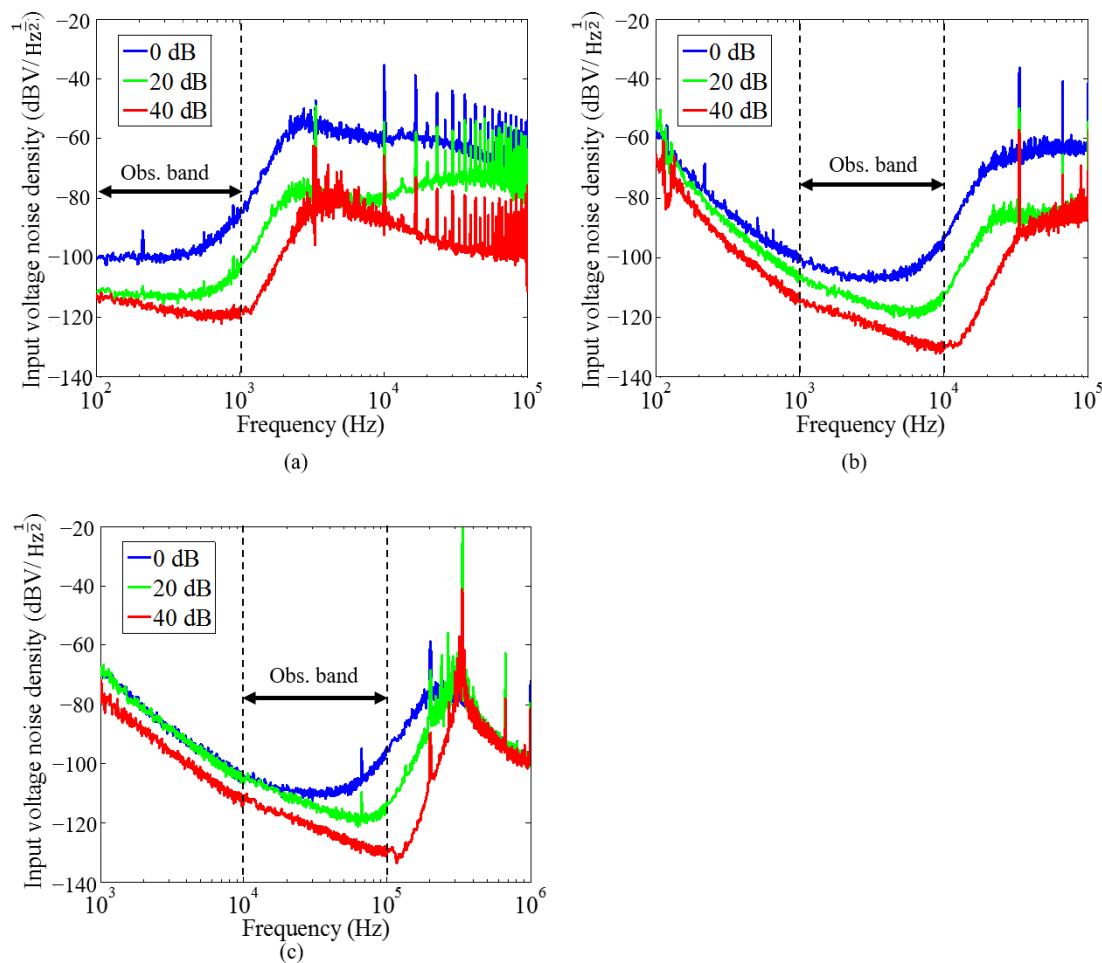**Figure 5: Circuit diagram of the noise elimination Gm-C LPF.**

5   **Figure 6: Layout of the ASIC for the spectrum receiver.**

Geoscientific
Instrumentation
Methods and
Data Systems
Discussions
Open Access

Figure 7: Typical frequency response performance of the ASIC in three observation frequency bands: (a) band 1 (1 Hz to 1 kHz), (b) band 2 (1 to 10 kHz), and (c) band 3 (10 to 100 kHz).

Figure 8: Input equivalent noise density of the ASIC for three observation frequency bands: (a) band 1 (1 Hz to 1 kHz), (b) band 2 (1 to 10 kHz), and (c) band 3 (10 to 100 kHz).
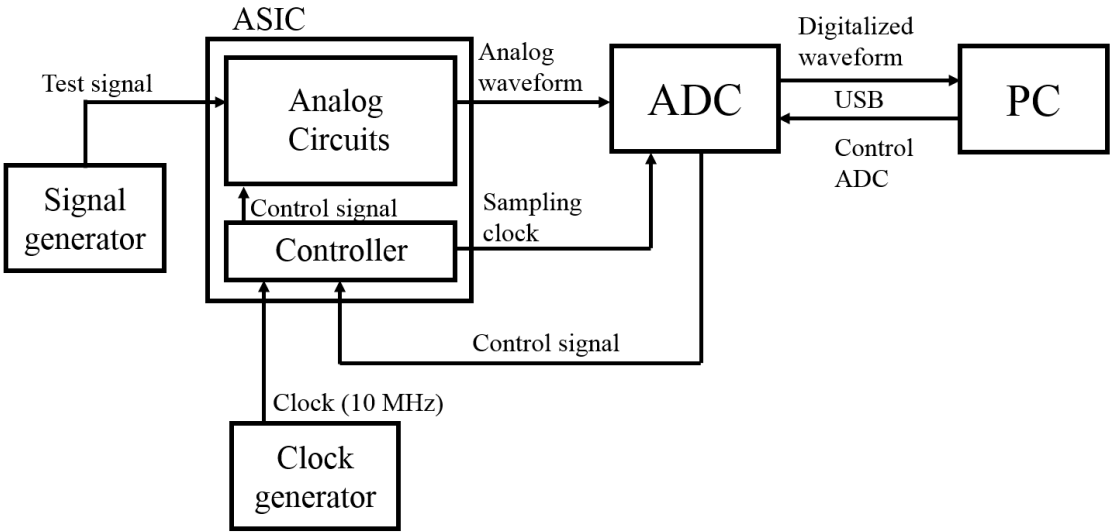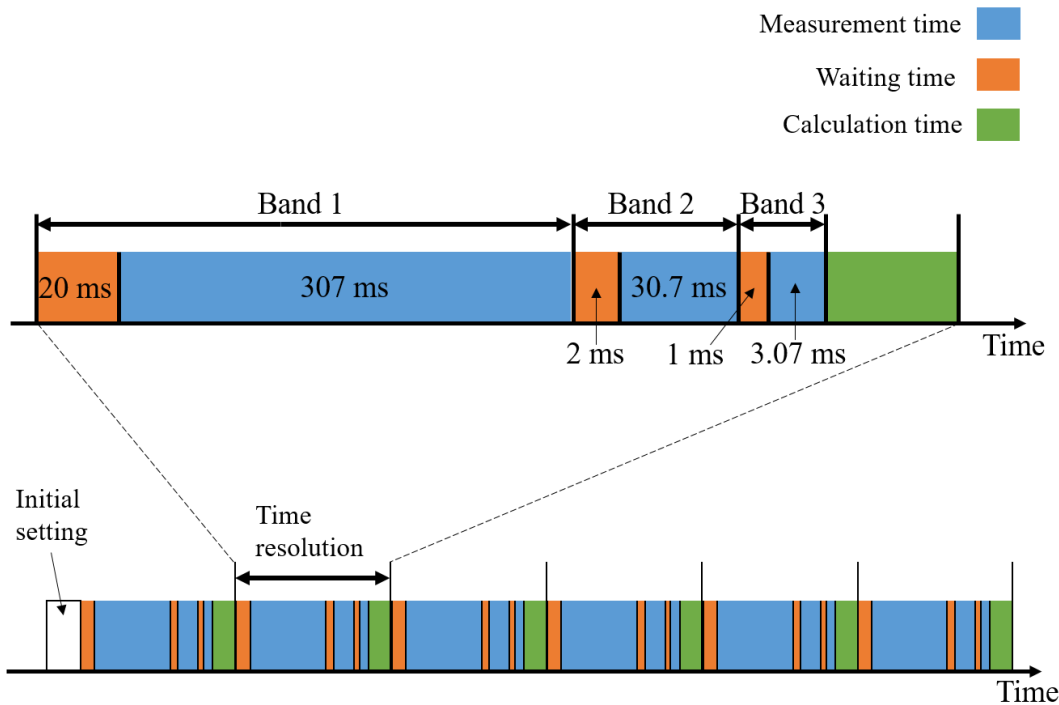
Figure 9: Test system for the proposed spectrum receiver.

5 **Figure 10: Measurement process for the receiver.**
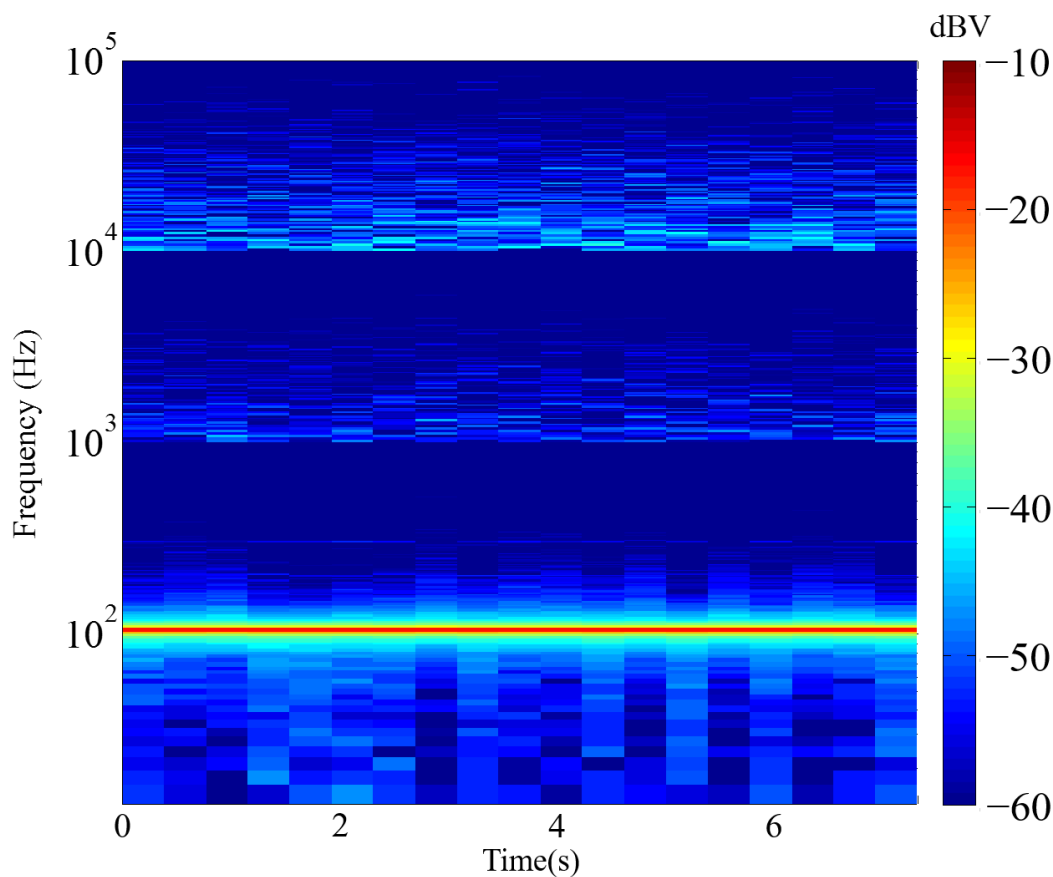
Figure 11: Observation results for the demonstration model.

Table 1: Correspondence of the capacitances and switch configurations to the cutoff frequency in the Gm-C HPF.

Cutoff frequency (kHz)	S_1, S_2	C_1 (pF)	C_2 (pF)
100	OFF	1	2
10	ON	12	22

5

10

Geoscientific
Instrumentation
Methods and
Data Systems
Discussions

Table 2. Capacitance of the SC LPF

	First stage	Second stage	Third stage
C_1 (fF)	25	25	25
C_2 (fF)	1125	1175	650
C_3 (fF)	25	25	25
C_4 (fF)	25	125	25
C_5 (fF)	1475	25	50
C_6 (fF)	1125	1175	650

Table 3. Correspondence of the capacitances and switch configurations to the cutoff frequency in the Gm-C LPF.

Cutoff frequency (kHz)	S_{11}, S_{21}	S_{12}, S_{22}	C_1 (pF)	C_2 (pF)
400	OFF	OFF	7.8	2.6
40	ON	OFF	78	26
4	OFF	ON	780	260
Not in use	ON	ON	-	-

5   **Table 4. Correspondence of the properties of each component to the observation band.**

Band no.	Band-limiting filters		Cutoff frequency of the antialiasing filter (kHz)	Sampling frequency (kHz)	Total frequency range (kHz)
	Filter type	Cutoff frequency (kHz)			
Band 1	LPF	100	1	3.3	0–1
Band 2	BPF	1, 100	10	33.3	1–10
Band 3	BPF	10, 100	100	333.3	10–100

Table 5. Observed gains for each band and gain setting.

Gain setting (dB)	Gain of band 1 at 0.5 kHz	Gain of band 2 at 5 kHz	Gain of band 3 at 50 kHz
0	−0.2	−1.6	−8.0
20	18.5	17.6	10.9
40	37.9	36.8	29.7

Geoscientific
Instrumentation
Methods and
Data Systems
Discussions

Table 6. Sampling times and frequency resolutions for each band.

Observation band	Measurement time (ms)	Frequency resolution (Hz)
Band 1 (1 Hz–1 kHz)	307	3.2
Band 2 (1–10 kHz)	30.7	32
Band 3 (10–100 kHz)	3.07	320